이학석사학위논문

Cell Surface Assembly of CD147 and CD276 Promotes Docetaxel Resistance in Breast Cancer

유방암에서 CD147과 CD276의 막단백질 집합체에 의한 항암제 저항성 기전에 대한 규명

2020년 02월

서울대학교 대학원

분자의학 및 바이오제약학과 전공

김 소 현

Cell Surface Assembly of CD147 and CD276 Promotes Docetaxel Resistance in Breast Cancer

Sohyun Kim
Department of Molecular Medicine and
Biopharmaceutical Sciences
Graduate school of Convergence Science and Technology
Seoul National University

Abstract

Integral plasma membrane proteins not only mediate responses to endogenous and environmental cues that regulate various cellular events, but they also maintain the intrinsic properties of cellular states. Here, we aimed to show that the lateral assembly of oncogenic proteins with CD147 and membrane expression of this assembly is integral to maintaining features of breast cancer stem cells. Utilizing proteomics with an anti-CD147 antibody probe, we discovered CD276 and other known cancer stem cell markers, such as CD44, CD133, and EGFR that are considered to be nearest neighbors of CD147. The cell surface assembly of CD147, CD276, and other oncogenic proteins was concealed within a lipid-raft-like microdomain. This finding was confirmed by confocal microscopy. Sequestration of this unique surface protein assembly confers resistance to docetaxel via an Akt-dependent p53-mediated apoptotic signaling pathway. In summary, the lateral interaction between CD147 and proximal partners promotes docetaxel resistance and suggests a key determinant of the cancer cell stemness phenotype.

Keywords: Basigin, Lateral organization, Proximity labeling, Chemo-resistance
Student Number: 2018-25475

ABBREVIATIONS

Ab	**Antibody**
ACN	**Acetonitrile, CH_3CN**
CAV-1	**Caveolin-1**
CD	**Cluster of Differentiation**
CD133	**Prominin-1**
CD147	**Basigin, EMMPRIN**
CD276	**B7-H3**
CD44	**Hyaluronate Receptor**
CSC	**Cancer Stem Cell**
DB	**Database**
DOC	**Docetaxel**
DTT	**Dithiothreitol**
EGFR	**Epidermal Growth Factor Receptor**
ESI	**Electron Spray Ionization**
FA	**Formic Acid, HCO_2H**
FDR	**False Discovery Rate**
GO	**Gene Ontology**
HCD	**High Collisional Dissociation**
HRP	**Horseradish Peroxidase**
IAA	**Iodoacetamide**
IPA	**Ingenuity Pathway Analysis**
LC-MS/MS	**Liquid Chromatography and Tandem Mass Spectrometry**
MBCD	**Methyl beta cyclodextrin**
MeOH	**Methanol**

NCS	**Normalized Collision Energy**
PAGE	**Poly Acrylamide Gel Electrophoresis**
PLGEM	**Power Law Global Error Model**
Q-Exactive	**Quadrupole-orbitrap Mass Spectrometer**
SDS	**Sodium Dodecyl Surfate**
STN	**Signal-to-noise ratio**
WB	**Western Blot**

Table of Contents

List of Tables

List of Figures

Introduction

Cell surface membranes are dynamic organelles that separate the interior of the cell from the extracellular space and consist of a lipid bilayer with embedded proteins. Membrane proteins are major components of plasma membranes and mediate responses to endogenous and environmental cues that regulate various cellular events[1]. In tumor microenvironments, the phenotype, functional heterogeneity, and bidirectional crosstalk among membrane proteins can lead to the formation of protein assemblies that are correlated with aggressive phenotypes.

The hallmarks of cellular plasticity and spatial heterogeneity critically affect cancer progression by regulating cancer stem cell (CSC) physiologies. The tumor microenvironment not only supplies growth-promoting signals, but it also takes part in therapeutic resistance by protecting tumor cells from the therapy-induced damage. The underlying mechanisms of tumor microenvironment interactions have been investigated to develop more effective cancer therapies. To gain a satisfactory understanding of the relationship between cancer cell heterogeneity and therapeutic resistance, a detailed study of the molecular organization of oncogenic proteins and the structure of such systems is needed[2].

CD147, also known as basigin (BSG) and extracellular matrix metalloproteinase inducer (EMMPRIN), is a cell surface membrane glycoprotein that is expressed at high levels on the surface of tumor cells[3]. Previous work revealed that the expression of CD147 protein was increased in CSC-like cells, and the functional consequences of CD147 overexpression suggest it plays a critical role in promoting chemoresistance and tumor cell survival[4]. More recent work has shown that CD147 induces the expression of vascular endothelial growth factor (VEGF)[5] and hyaluronan (HA), proteins that facilitate metastasis and multidrug resistance[6], respectively. However, CD147 has functions other than matrix metalloproteinase induction and most likely

acts as a functional binding partner for several plasma membrane proteins, including EGF receptors, CD133, and the hyaluronan receptor CD44, thereby influencing activities characteristic of cancer stem-like cells, such as cell survival and drug resistance. In addition, CD147 localizes to discrete membrane microdomains, referred to as lipid rafts. Moreover, recent studies have shown that CD147 promotes the assembly of signaling complexes containing CD133, CD44, and EGFR in lipid-raft-like microdomains that typically promote survival or tumor initiation[7,8]. These findings indicate that CD147 is an important regulatory molecule in tumor progression and presenting resistance to chemotherapy, making it an attractive target for anticancer treatments[9]. However, the mechanisms by which CD147 activates signaling cascades are not fully understood.

Several studies have identified molecules with which CD147 interacts by conventional affinity purification coupled with mass spectrometry (AP-MS). However, these approaches have shortcomings. For example, conventional affinity purification requires detailed knowledge of the binding specificity of CD147 to the interacting partners so that the functional group used in the affinity purification does not interfere with the binding interaction. Recently, enzyme-catalyzed proximity labeling approaches have been developed to identify the lateral composition of CD147. AP-MS uses biochemical isolation of intact protein complexes, but proximity labeling is performed in living cells in the native cellular environment. Consequently, proximity labeling enables the identification of weak and transient interactions, which are typically disrupted during affinity purification experiments.

Therefore, mapping interaction networks outward from CD147 to proteins that interact with CD147 within the membrane would reveal how the proteome is organized into functional units. Such information is important for understanding the complex biological processes that lead to drug-resistance. To identify the composition of proteins that are nearest to CD147 in cancer stem cell membranes, I adapted

proximity labeling assays based on the tyramide radicalization principle[10-14]. For our model, I used a CSC-like cell line derived from MDA-MB453 breast cancer cells. The cells were generated by Sajithlal and colleagues by transfecting green fluorescent protein under the control of the human octamer binding transcription factor 3/4 (Oct3/4) promoter into the MDA-MB453 breast cancer cell line[15]. For proximity labeling, a peroxidase enzyme targeted to CD147 reacts with a substrate to generate short-lived products that covalently label proteins in the vicinity of the CD147. The labeled proteins can then be identified by mass spectrometry. This proximal labeling method[12] allows the proteins that co-assemble with the CD147 in the plasma membrane of cancer stem cells to be selectively biotinylated, which facilitates their isolation for mass spectrometry. I identified known and novel components of the CD147 nearest-neighbor proteomes and localized the assembly to the lipid-raft-like microdomain where CD147 is co-assembled with other proximal molecules that have been implicated in the cancer stemness phenotype.

Interestingly, we detected CD276 (B7-H3), an immune checkpoint protein that is expressed in antigen-presenting cells (APCs) and macrophages to regulate the function of T cells as a second signal molecule[16-19], but whose function is still unknown in cancer cells. I show that CD276 resides in lipid-raft microdomains in the CSC-like cell membrane and investigate the oncogenic lateral interactions by disrupting the lipid-raft compositions with a contributing mechanism to docetaxel (Doc)[20]. Consistent with this view, we showed that the co-localization of CD147 and CD276 is a key determinant of the drug resistance phenotype in CSC, making it an attractive target for anti-tumor treatments. This study aims to examine the mechanism that facilitates co-assembly of CD147 with proximal partners in CSCs and report a mechanistic approach to overcome resistance to docetaxel.

2. METHODS

2.1 Cell culture

CSC-like MDA-MB453 cells and non-CSC-like MDA-MB453 cells were obtained from the University of Pittsburgh Medical Center (Pittsburgh, Pennsylvania, USA)[15]. In addition, CD147 Knockout cells by CRISPR-Cas9 were received from Kangwon University. Cells were grown at 37℃ in an atmosphere of 5% CO_2 in DMEM containing 10% Fetal bovine serum (FBS) (HyClone, Logan, UT) and 1% penicillin/streptomycin. ‘

2.2 Reagents and antibodies

HPLC grade acetonitrile (ACN), HPLC grade water, formic acid (FA), urea, dithiothreitol (DTT), iodoacetamide (IAA), and ammonium bicarbonate were purchased from Sigma-Aldrich (St. Louis, MO, USA). Sep-pak C18 cartridges were obtained from Waters (Milford, MA, USA). Trypsin protease MS-grade was from Thermo Scientific (Rockford, IL, USA). Antibodies against CD147 (2B9, mouse monoclonal) and CD44 (3C7. Mouse, monoclonal) was home-made, GAPDH (15C10, rabbit monoclonal) primary antibody are supplied from Cell signaling Technology (Danvers, MA). Antibodies against CD133 (C1C2, rabbit polyclonal) was from genetex. Antibodies against CD276 (AF1027, goat polyclonal) was from R&D systems. Antibodies against MCT4 (sc-376101, mouse monoclonal) was from santa cruz. Anti-rabbit and anti-mouse secondary antibodies were purchased from AbFrontier company (Young In Frontier, Seoul, Korea).

2.3 Synthesis of Tyramide-SS-Biotin and HRP-conjugated anti CD147

The synthesis of cleavable tyramide-biotin label was prepared by gently mixing 5mg of EZ-Link-biotin label (Thermo) with 1.55mg of tyramide hydrochloride (Sigma) in

100ul dimethyl sulfoxide and put it into 2mL 1X PBS, overnight, at room temperature in the dark[13]. After filtering with a 2mL disposable syringe the tyramide-biotin was stored at -20℃.

2.4 Preparation of CD147-Fc fusion protein

Coupling of HRP to CD147 antibody has been carried out using EZ-Link™ Plus Activated Peroxidase kit (Thermo). Human IgG antibody was coupled with HRP and used as a negative control.

2.5 Biotin Labeling of CD147 proximal proteins by Tyramide radicalization and affinity purification of biotinylated proximal proteins

For proximity labeling, cells ($2x10^8$) were washed three times with cold PBS and incubated with HRP-CD147 Ab and HRP-HuIgG for 2 hours at 4℃ with shaking respectively. After incubated, cells were washed three times with cold PBS and biotinylated by tyramide labeling buffer for 15 minutes. After that, cells were washed three times with cold PBS and HRP-Abs were stripped by antibody strip buffer at room temperature and washed again. Cells were lysed by RIPA lysis buffer (Thermo) and sonicated with sonication on ice. Protein concentrations of the total cell lysates were measured using a BCA Protein Assay kit (Thermo Scientific). Biotinylated proximal proteins were isolated using a Streptavidin Magnetic Beads (Thermo Scientific, Pierce) following the manufacturer's protocol. The protein concentrations of the column eluents were determined by NanoDrop.

2.6 One-dimensional SDS-PAGE fractionation and In-gel digestion

Equal amounts of total protein were resolved and loaded. The isolated protein samples were fractionated by sodium dodecyl sulfate polyacrylamide gel electrophoresis (SDS-PAGE) with 4~ 12% Bis-Tris Gel (Bolt MOPS running buffer) (Invitrogen,

Carlsbad, CA, USA) and stained with Instant Blue (Sigma Aldrich). Each gel lane was cut into seven pieces and subjected to in-gel tryptic digestion following the general protocol (Shevchenko et al. 2006). Briefly, protein bands were excised, destained, and washed. Proteins were reduced with 20mM DTT at 60°C for one hour and alkylated with 55mM iodoacetamide at room temperature for 45 minutes in the dark condition. After dehydration, the proteins were digested with 13ng/uL sequencing-grade modified porcine trypsin (Promega, Madison, WI) in 50mM ammonium bicarbonate overnight at 37°C. Peptides were extracted from the gel slices with 50% v/v ACN in 0.1% v/v formic acid, and 80% v/v ACN in 0.1% v/v formic acid, and dried under vacuum.

2.7 Mass Spectrometry Analysis and Database Search

Peptides were resuspended in 20μL Solvent A (0.1% formic acid in water) and 9μL sample was loaded onto an analytic column (PepMap, 75 μm ID*50 cm 3 μm, ES803, Thermo Fisher Scientific) and separated with a linear gradient of 5-32% Solvent B (0.1% formic acid in ACN) for 90 min at a flow rate 300nL/min. Samples were analyzed in duplicate on a Q-Exactive (Thermo Fisher Scientific, San Jose, CA) hybrid quadrupole-Orbitrap mass spectrometry, interfaced with a HPLC system. The voltage of the spray was set to 2.2kV and the temperature of the heated capillary was set to 250°C. The full scans were acquired in the mass analyzer at 400-1400m/z with a resolution of 70,000 and the MS/MS scans were obtained with a resolution of 17,500 by normalized collision energy of 27eV for high-energy collisional dissociation fragmentation. The advanced gain control target was 5 × 104, maximum injection time was 120 ms, and the isolation window was set to 3 m/z. The Q-Exactive was operated in data-dependent mode with one survey MS scan followed by ten MS/MS scans, and the duration time of dynamic exclusion was 60 s.

2.8 Database search for protein identification and functional analysis

Collected MS/MS data were converted into mzXML files through the Trans Proteomic Pipeline (version 4.5) software and searched against the decoy Uniprot Human database (version 3.83, 186 578 entries) for the estimation of false discovery rate with the SEQUEST® (Thermo Fisher Scientific; version 27) program in the SORCERER™ (Sage-N Research, Milpitas CA, version 3.5) search platform. Precursor and fragment ion tolerance were set to 10 ppm and 0.5 Da, respectively. Trypsin was chosen as the enzyme with maximum allowance of up to two missed cleavages. Carbamidomethyl of cysteine was considered as the fixed modification, a differential modification on methionine oxidation. The Scaffold software package (version 3.4.9, Proteome Software Inc. Portland, OR) was used to validate MS/MS-based peptide and protein identification. Peptide and protein identification were accepted if they could be established at greater than 95 and 99% probability, respectively, as specified by the Peptide and Protein Prophet algorithm, and if the protein identification contained at least two identified peptides with a false discovery rate <0.1%.

2.9 Identification of proximal proteins nearby CD147 and Quantification of relative proteins and bioinformatics analysis

Identified proximal proteins nearby CD147 were accomplished using spectral counting. The MS/MS data were normalized to compare the abundances of proteins between samples using Scaffold software. The normalized spectral counts from duplicate analyses of the CSC-like/non-CSC(NCSC)-like cells were compared using the R program with power law global error model (PLGEM) software in order to identify statistically significant protein changes between the two cell. The subcellular localization and functional annotation of identified proteins were classified using Ingenuity Pathway Analysis (Ingenuity Systems.) and PANTHER (Protein Analysis

Through Evolutionary Relationships) Classification System (v7.2). The potential protein-protein interactions and networks of the identified proteins were annotated by IPA analysis.

2.10 Isolation of Lipid Rafts

Membrane lipid rafts were isolated as described previously. The isolation protocol was followed by Macdonald and pikes' protocol. Briefly, 3x 10^7cells cultured and washed with ice-cold PBS three times. Cells were lysed in 1ml of lysis buffer (10mM Tris-HCl, pH7.4, 1mM EDTA, 200mM sucrose, 1X protease inhibitor mini tablet (Pierce, Cat#88665), on ice for 30 min and pelleted down with 14,000 x g for 30 min to obtain only the membrane part. Then, change the buffer to 1.2ml of lysis buffer including 1% Triton X-100 and mechanically disrupted by probe sonication for 5 mins each and incubate on ice for 30 min. The lysates were mixed directly with iodixanol stock solution (60% solution of Optiprep iodixanol) to yield a 40% (v/v) iodixanol-lysate solution, which was placed at the bottom of an ultracentrifuge tube. Equal volumes of 0-20% Opti-prep in lysis buffer without Triton X-100 were carefully overlaid above the iodixanol-lysate solution. The samples were centrifuged at 200,000 x g for 4 h at 4 °C in a SW41 Ti rotor (Beckman Coulter). Fractions of 1ml (typically 11-12 fractions in total) were collected from the top of the gradient tube. All buffers from fractions were exchanged into 1x PBS to remove iodixanol solution. Fractions, containing rafts were pooled, were separated via SDS-PAGE, transferred to PVDF membrane and immunoblotted utilizing antibodies to confirm the fractions containing lipid-raft microdomains and recognize proteins of interest.

To destroy the lipid raft structure, cholesterol, the structural base of the lipid raft, was removed. Briefly, cells were washed in PBS to remove serum. Cells were incubated in DMEM containing 5mM Methyl-beta-cyclodextrin (MBCD, Sigma-Aldrich) for 2hr at 37°C. Cells were fractionated as described above.

2.11 ㄴ Establishment of CSC knock-out cell lines

The CRISPRv2 vector system was obtained from Addgene (Cambridge, MA, USA, #52961) to deliver Cas9, a sgRNA, and a selective marker (puromycin) into target cells. Lentiviruses were produced by transducing CSC cells with lentiCRISPRv2 plasmids (*CD147, CD44, CD133, DBKO* (*double CD147, CD44*), TPKO (*triple CD147, CD44* and *CD133)*, and *CD276*. A mixture of 30µg of each gRNA-Cas9 plasmids was transfected into CSCs ($1x10^6$ cells) through electroporation at 160V and 500uF using GenePulser Xcell™ (BioRad). The tdTomato positive cells were isolated by FACS Aria (BD), and then single cell clonal selection was performed by limiting dilution in 96-well plates and clonal expansion. both knock-out were confirmed by Flow cytometry and Western blot analyses.

2.12 Mode of Treatment

In all combination treatments, methyl-beta cyclodextrin (5mM) was added 2h before Docetaxel (25nM) treatment. The DMSO concentration in all experiments, including controls, was <0.2%.

2.13 Western Blot Analysis

Whole lysates were prepared for immunoblotting using a RIPA lysis buffer. Protein content was quantified using a BCA assay (Pierce), and aliquots were solubilized in non-reducing sample buffer, resolved on Bolt™ 4-12% Bis-Tris Plus polyacrylamide gels, transferred to PVDF, blocked in 5% nonfat dry milk or 3% BSA with Tris-buffered saline and 0.1% Tween 20, and stained with primary antibodies, HRP-linked secondary antibodies were detected with ECL, and sizes of proteins were estimated

from molecular weight standards electrophoresed on the same gel as the samples. For lipid raft isolation, 20ug of samples were loaded and for signaling assay, 40ug of samples were loaded respectively.

2.14 Cell Viability Assay

The Cells viability was carrying out using the Enhanced Cell viability assay EX-Cytox (water-soluble tetrazolium salt method). The absorbance (A450) of each well was measured using a Power Wave X. EZ-Cytox assay (dehydrogenase assay): 5 X 10^4 cells per ml, the WST reagent solution was added to each well of a 96-well microplate that contained 100 ul of cells in the growth medium under control conditions (96 wells for cell culture). The plate was then incubated for 1 h at 37°C. The absorbance was measured at 450 nm using a microplate reader. At the same time, growth medium without cells were incubated for 1 h to obtain the background signal. As a result, we were able to calculate the final value: (total signal – background signal = original signal -> (original signal / control signal) = relative proliferation).

2.15 Immunofluorescence Imaging

Cells grown on coverslips were fixed with 2% paraformaldehyde in PBS at room temperature for 10 minutes, rinsed with PBS, and treated with 1.5mg/ml glycine in PBS to quench free aldehyde groups. Cells were then stained either with Texas Red-Streptavidin for biotin staining or with anti-CD147- Alexa 647 for CD147 on membrane. For nucleus staining, cells were incubated with DAPI(0.5ug/ml). After washing with PBS, cells were examined using Carl Zeiss fluorescence microscopy. For biotin stripping, 5mM TCEP in 150mM NaCl, 1mM EDTA, 0.2% BSA, 20mM Tris, pH 8.6 was added.

2.16 Cell Cycle Analysis

Cells were trypsinized, washed, and resuspened in 1mL PBS. Subsequently, cells were washed twice with icd-cold PBS and then 66% (v/v) ethanol was added to fix the samples. After centrifugation, cells were digested with RNase A (500U/mL) for 30 min at 37°C and stain with propidium iodide (50ug/mL). The DNA content (10,000 cells per experimental group) was determined using a FACS Calibur flow cytometer (Becton Dickinson Biosciences, San Jose, CA, USA) equipped with a ModFit LT program (Verity Software House, Topsham, ME, USA), as previously described. At least 18000 events were measured for each sample.

2.17 Statistical Analysis

All statistical analyses were performed using GraphPad Prism 8 (GraphPad, CA, USA). Results are as the means ± standard error of the means (SEM). Differences between two groups were assessed by Student t-test. The error bars represent +_ S.D of the experiments. The statistical analysis was carried out using student t-test. ***, **, * and ϕ represents P-values ≤0.0001, ≤0.001, ≤0.005 and >0.05, respectively.

3. RESULTS

3.1 Analysis of CD147 proximal surface proteins in CSC cells

Association between CD147 and resistance phenotype to anti-cancer therapeutic reagents in tumor has been extensively studied. To characterize the surface protein assembly in the vicinity of CD147 expressed on CSC, we used the selective proteomic proximity labeling method **(Figure 1A and 1B)** using a HRP conjugated anti-CD147 Ab and a HRP conjugated anti-IgG Ab (negative control) with the tyramide-biotin reagent (**Figure 2A and 2B)**. Prior to identification of CD147 proximal proteins, we conducted an immunofluorescence imaging analysis to ensure the cell surface biotin labeling incurred by the HRP conjugated anti-CD147 Ab. Overlapping immunofluorescence images of CD147 and biotinylation in CSC and NCSC demonstrated that cell surface of CSC appeared to be prevalently biotinylated than NCSC **(Figure 3A and 3B)** which correlates with higher expression levels of CD147 in CSC. Stripping biotins by reducinng the disulfide linkage of cell surface bound biotinylated molecules on CSCs proved that the overlapping immunofluorescence image was incurred by the biotin deposition **(Figure 3C)**. We then sought to identify uniquely assembled proximal proteins near CD147 in CSC by incubating the HRP conjugated anti-CD147 Ab with an equal number of CSC and NCSC cells ($2x10^7$ cells). After biotin deposition, biotinylated CD147 proximal proteins were isolated by streptavidin purification and an equal amount of proteins (100ug of each) of CSC and NCSC was fractionated by SDS-PAGE gel **(Figure 4A)** and subjected to in-gel tryptic digestion. Duplicate LC-MS/MS analysis identified a total of 528 proteins (at least two unique peptides with false discovery rate (FDR) $\leq$1%) in CSC and NCSC by the protein database search **(Figure 4B)**. Label-free quantitative analysis provided 200 differentially expressed proteins in both cell lines (PLGEM-STN p-value < 0.001) **(Figure 4C and Table 1).** Hierarchical clustering showing the spectral counts of high confidence interactors (p-value <0.01 after PLGEM-STN analysis) identified with HRP conjugate CD147 or IgG are shown. CD276 and SLC16A3 (MCT4) were the only interactors unique to negative control. On the right, Gene Name, STN are shown **(Figure 4D)**. To validate the data, we performed the protein-protein interaction network analysis of 55 proteins with STRING tool which exhibited the majority of proteins are known to be associated with CD147 **(Figure 5A)**. Functional annotations in the reactome pathways of CD147 proximal proteins in CSC indicated that their molecular associations with CD147 (Basigin interactions) **(Figure 5B)**. **Figure 6A-F** shows the representative QE MS/MS spectra of in-gel digested peptides of lateral organization of CD147 in CSC-like cell specific bands. Those peptides were

selected by criteria which contain accordance of molecular weight on identified protein with distinguishable band, uniqueness on the identified protein, meaningful signal intensity, and the total number of fragment ions.

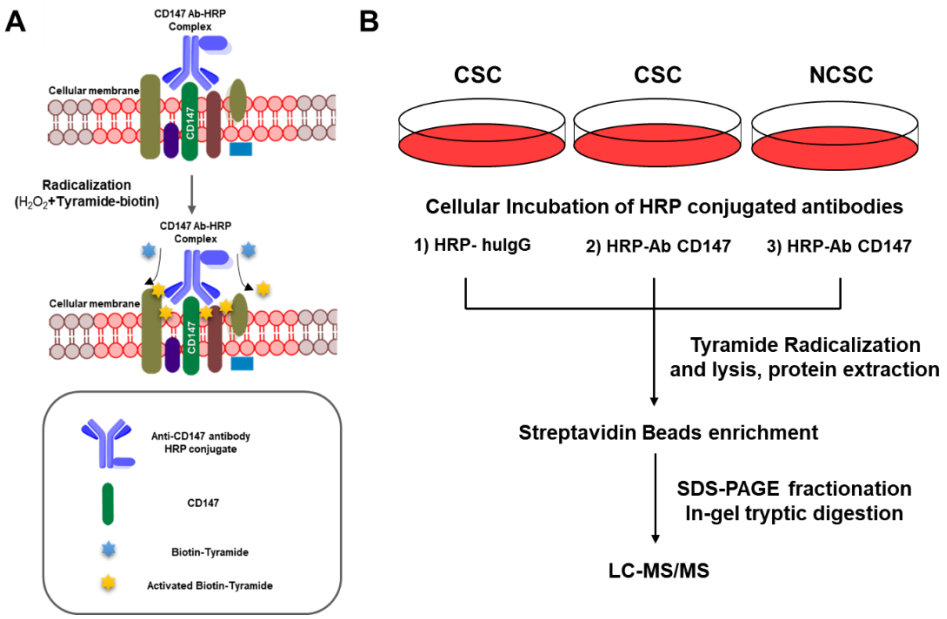

Figure 1. Outline of experimental strategies for the proximity labeling of CD147 using the tyramide radicalization principle. (A) Principle of the proximity labeling method**.** The CD147 antibody conjugated with HRP are incubated and react with hydrogen peroxide and biotin-tyramide to generate the radicals that covalently label the proteins in vicinity of CD147. **(B)** The whole proteomic process of the method**.** These biotinylated proteins are isolated by streptavidin beads, and eluted with DTT treatment and subjected to in-gel digestion and LC-MS/MS for identification.

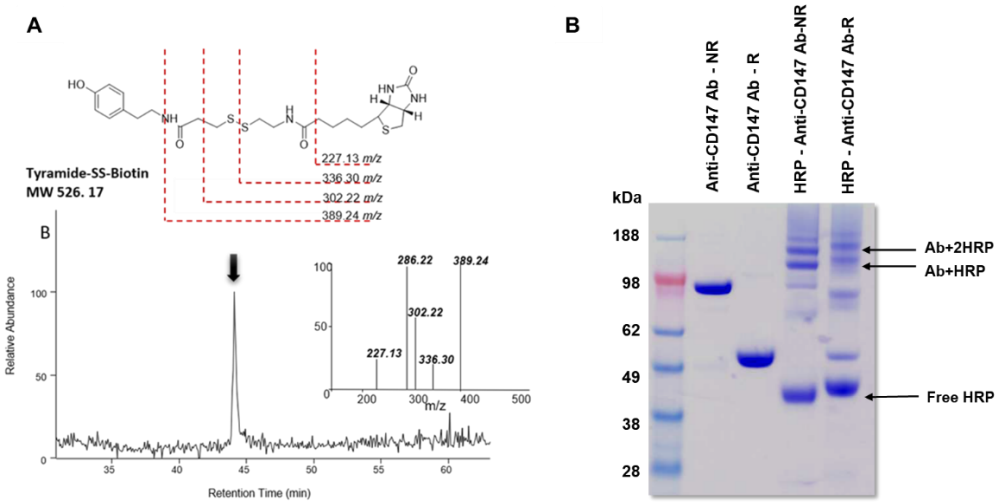

Figure 2. Validation of the synthesis of tyramide-SS-biotin and HRP-conjugated anti-CD147 to be used for proximity labeling. (A) A structure and LC-MS/MS spectra and structural elucidation of Tyramide-SS-biotin (m/z 526.17). **(B)** SDS-PAGE analysis of HRP-conjugated CD147 antibodies. Equal amounts (20ug) of conjugated and purified HRP-conjugated CD147 antibodies were analyzed by SDS-PAGE under reducing and non-reducing conditions (8-12% gradient gel).

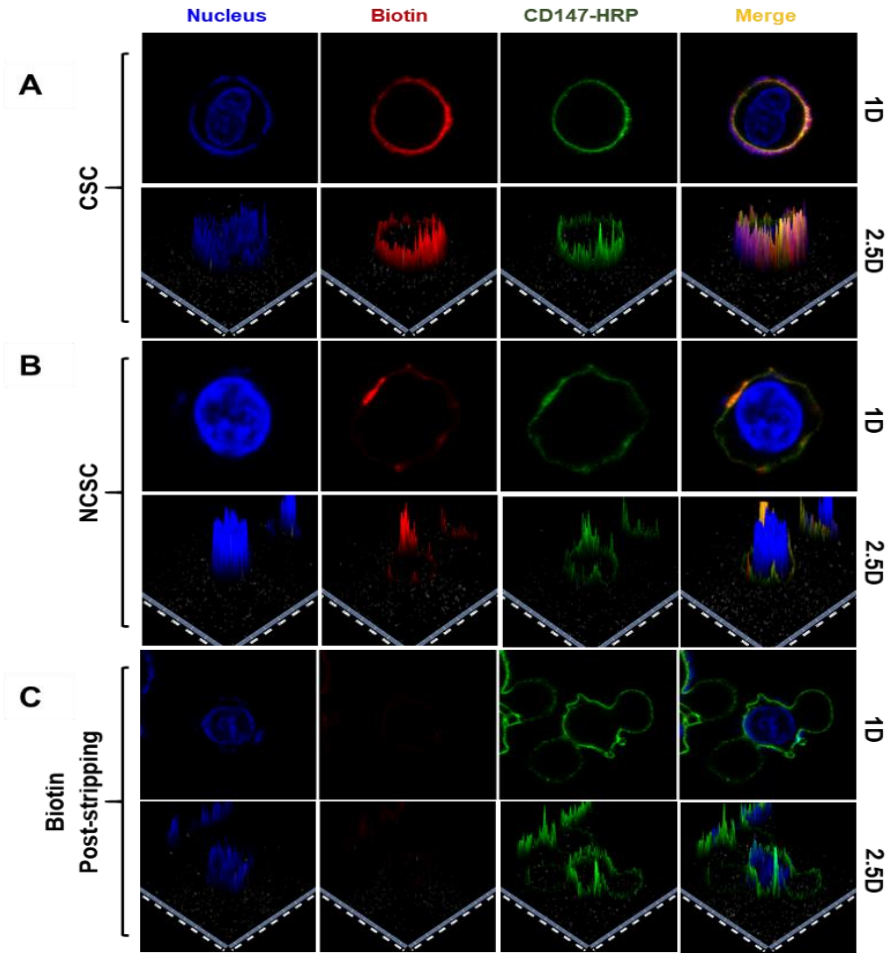

Figure 3. Confocal immunofluorescence imaging of biotin deposition of cell surface proteins by a HRP-conjugated anti-CD147 Ab probe. (A) 1D (upper panel) and 2.5D* (under panel) immunofluorescence images of biotinylated cell surface proteins (red) and CD147 (green) of CSCs, and **(B)** non-CSCs. The specific co-staining was apparent in the merged images (biotin and CD147) are shown as yellow/orange in the cell surface. **(C)** Deposited biotin labels were stripped by TCEP treatment as described in the Material and Methods. All confocal dishes were fixed and stained with Alexa647 conjugated F(ab')2 Goat anti-huIgG to detect CD147, and streptavidin, Texas Red-X conjugate to detect deposited biotinylated proteins.

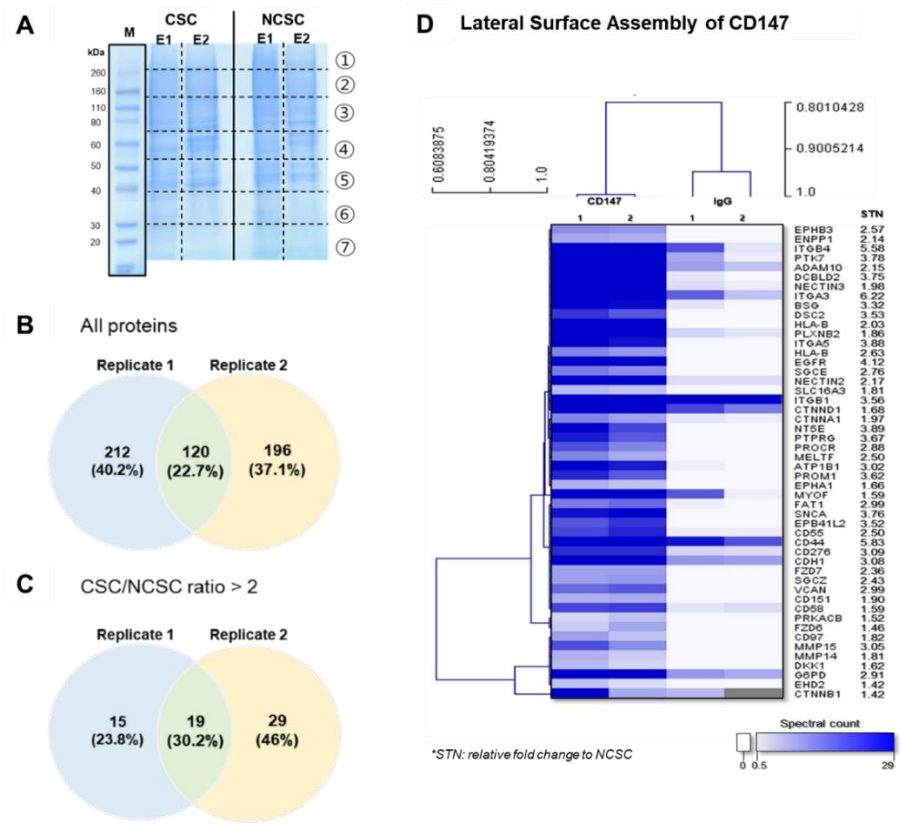

Figure 4. Identified proximal proteins near CD147 in CSC and NCSC. (A) After NanoDrop, 100ug of total protein was loaded and separated by preparative Bolt^{TM} 4-12% Bis-Tris gel. Stained with Instant Blue, seven gel band regions were excised and subjected to an in-gel digestion with trypsin. Lane 1 molecular weight marker, lane 2 and 3; First and second elution on biotinylated proximal proteins of CD147 in CSC. lane 4 and 5; First and second elution on biotinylated proximal proteins of CD147 in non-CSC. **(B)** Venn diagram of identified proteins with differentially expressed proteins in each pair of samples and **(C)** Number of proteins twice or more abundant in the samples with CD147-HRP in CSC than Non-CSC. **(D)** Heatmap showing the spectral counts of high confidence interactors (*p-value <0.01*) identified with HRP conjugate CD147 or IgG are shown. CD276 and SLC16A3 (MCT4) were the only interactors unique to negative control. On the right, Gene Name, STN are shown.

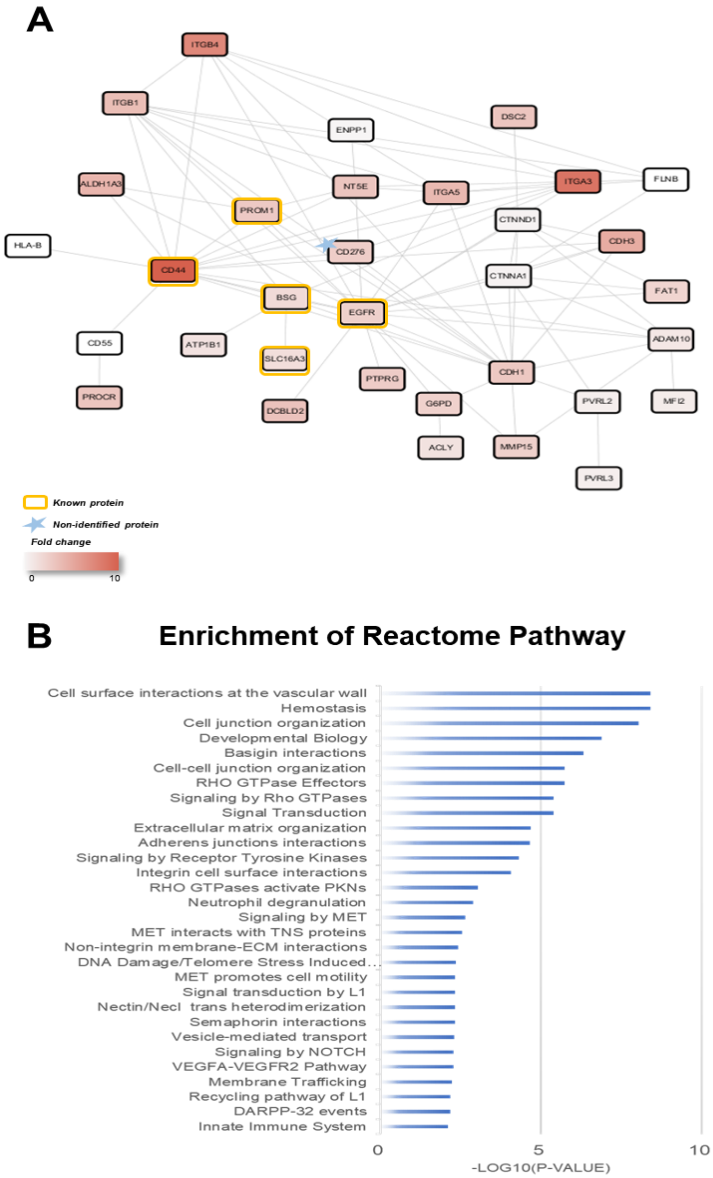

Figure 5. Functional analysis of surface assembly of CD147 proximal proteins near CD147 in CSC. (A) 55 proximal proteins of CD147 in CSCs, we categorized into biological process using STRING database tool. Those proteins were visualized as color representation with fold-change values of STN. **(B)** The most notable 10 of 99 REACTOME pathways of CSC-specific CD147 proximal proteins.

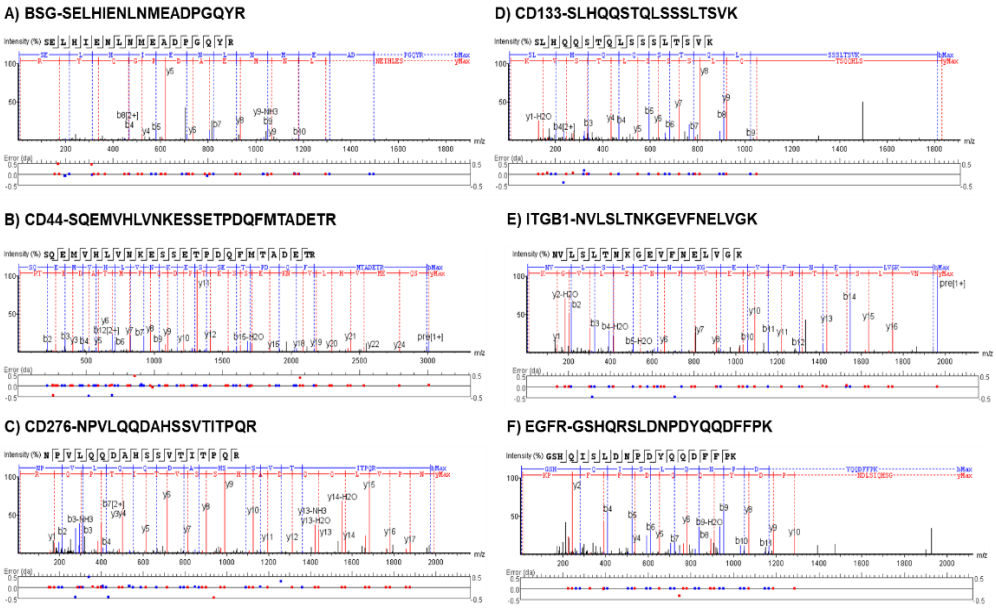

Figure 6. Tandem mass spectra of the peptides in the CSC-like cell specific proximal partners of CD147 detected by LC-MS/MS. (A-F) MS/MS spectra of the peptides, SELHIENLNMEADPGQYR, SQEMVHLVNKESSETPDQFMTADETR, NPVLQQDAHSSVTITPQR, SLHQQSTQLSSSLTSVK, NVLSLTNKGEVFNELVGK, GSHQRSLDNPDYQQDFFPK that represent CD147, CD44, CD276, CD133, ITGB1 and EGFR. Criteria of these peptides selection are the identified proteins' molecular weight accordance about distinguishable band, uniqueness on corresponding proteins, significant signal intensity, and the total number of fragment ions. Red and blue colors present the b fragment ions and y fragment ions, which were assigned by protein database search. The asterisk indicates unique peptide corresponding identified proteins.

Table 1. Identified CD147 proximal proteins from the CSC-like and Non CSC-like cells.

				Spectral Counts							
				Negative P* in CSC		CD147 P.P* in CSC		CD147 P.P* in NCSC			
No.	Accession	Protein Name	Gene Symbol	Ig1	Ig2	C1	C2	N1	N2	STN	p-value
1	P05556	Integrin beta-1	ITB1	92	47	347	326	164	210	4.565705	0
2	P0DOX5	Immunoglobulin gamma-1 heavy chain	IGG1	71	48	364	319	117	170	6.369795	0
3	P16070	CD44 antigen	CD44	55	28	277	257	51	62	8.741189	0
4	P15311	Ezrin	EZRI	49	23	126	99	152	184	-2.34351	0.000343
5	P06756	Integrin alpha-V	ITAV	44	17	103	98	160	225	-3.82605	0
6	O00159	Unconventional myosin-Ic	MYO1C	43	18	111	95	170	230	-3.9652	0
7	P13637	Sodium/potassium-transporting ATPase subunit alpha-3	AT1A3	34	24	93	81	69	64	1.186916	0.008751
8	O75369	Filamin-B	FLNB	39	13	101	89	24	39	4.206667	0
9	P08195	4F2 cell-surface antigen heavy chain	4F2	27	21	78	67	97	120	-1.9159	0.001287
10	Q9Y624	Junctional adhesion molecule A	JAM1	36	11	159	155	110	136	1.432564	0.004547
11	P01859	Immunoglobulin heavy constant gamma 2	IGHG2	27	14	227	203	42	71	7.115859	0
12	P01860	Immunoglobulin heavy constant gamma 3	IGHG3	29	12	216	191	42	69	6.795723	0
13	P01861	Immunoglobulin heavy constant gamma 4	IGHG4	28	12	165	138	40	74	4.774735	0
14	P01764	Immunoglobulin heavy variable 3-23	HV323	23	16	111	102	39	45	3.889067	0
15	Q86X29	Lipolysis-stimulated lipoprotein receptor	LSR	20	19	112	105	73	85	1.538083	0.003861
16	P01768	Immunoglobulin heavy variable 3-30	HV330	22	16	103	90	33	43	3.716937	0
17	P0DP03	Immunoglobulin heavy variable 3-30-5	HV335	22	16	103	90	33	43	3.716937	0
18	P26006	Integrin alpha-3	ITA3	22	15	301	277	74	90	7.842152	0
19	O60716	Catenin delta-1	CTND1	21	15	76	72	42	41	2.20408	0.000686
20	Q14118	Dystroglycan	DAG1	25	10	55	52	97	116	-3.03843	8.58E-05
21	Q9H5V8	CUB domain-containing protein 1	CDCP1	25	9	91	78	54	73	1.239882	0.008236
22	P01892	HLA class I histocompatibility antigen A-2 alpha chain	1A02	20	13	83	81	101	114	-1.32099	0.007207
23	P18084	Integrin beta-5	ITB5	25	4	54	33	57	92	-2.07593	0.000944
24	Q9Y5Y6	Suppressor of tumorigenicity 14 protein	ST14	16	10	59	49	75	92	-1.81676	0.001802
25	P16144	Integrin beta-4	ITB4	21	4	226	189	43	67	6.965601	0
26	P53396	ATP-citrate synthase	ACLY	18	5	60	46	15	24	2.960457	8.58E-05
27	Q9NZM1	Myoferlin	MYOF	18	5	76	73	39	58	1.697978	0.002574

28	P12830	Cadherin-1	CADH1	13	8	64	51	11	15	4.112876	0
29	P30443	HLA class I histocompatibility antigen A-1 alpha chain	1A01	13	8	74	73	46	55	1.493676	0.004204
30	P30455	HLA class I histocompatibility antigen A-36 alpha chain	1A36	13	8	75	74	48	56	1.445372	0.004547
31	P26038	Moesin	MOES	13	8	60	45	73	106	-2.2466	0.000515
32	P11413	Glucose-6-phosphate 1-dehydrogenase	G6PD	11	9	60	41	10	15	3.704477	0
33	O14672	Disintegrin and metalloproteinase domain-containing protein 10	ADA10	12	8	75	66	27	39	2.71389	8.58E-05
34	P01772	Immunoglobulin heavy variable 3-33	HV333	10	8	77	64	21	24	3.749149	0
35	A0A0C4DH42	Immunoglobulin heavy variable 3-66	HV366	10	8	74	63	21	25	3.57397	0
36	P10321	HLA class I histocompatibilituuuuuuy antigen Cw-7 alpha chain	1C07	10	7	35	37	50	66	-1.65813	0.002917
37	P01700	Immunoglobulin lambda variable 1-47	LV147	8	7	24	28	10	13	1.798362	0.001802
38	Q29963	HLA class I histocompatibility antigen Cw-6 alpha chain	1C06	9	6	44	42	58	72	-1.53827	0.004032
39	P30464	HLA class I histocompatibility antigen B-15 alpha chain	1B15	9	5	52	50	36	37	1.131031	0.009695
40	Q96S97	Myeloid-associated differentiation marker	MYADM	9	5	29	26	42	51	-1.62723	0.002917
41	P29508	Serpin B3	SPB3	8	5	56	39	2	4	5.374431	0
42	O15031	Plexin-B2	PLXB2	9	4	142	109	75	108	1.641016	0.002745
43	P29323	Ephrin type-B receptor 2	EPHB2	9	4	31	23	58	83	-3.28042	0
44	Q13308	Inactive tyrosine-protein kinase 7	PTK7	10	2	96	93	26	42	3.956654	0
45	Q6YHK3	CD109 antigen	CD109	10	2	29	20	70	102	-4.41591	0
46	P30499	HLA class I histocompatibility antigen Cw-1 alpha chain	1C01	6	5	27	24	44	53	-1.97783	0.001287
47	Q5ZPR3	CD276 antigen	CD276	6	4	28	27	3	2	3.874579	0
48	Q8NFZ8	Cell adhesion molecule 4	CADM4	6	4	40	34	13	16	2.374074	0.000172
49	Q92485	Acid sphingomyelinase-like phosphodiesterase 3b	ASM3B	7	3	18	25	6	12	1.73356	0.002402
50	Q92692	Nectin-2	NECT2	7	3	50	39	10	28	2.398655	8.58E-05
51	Q7L576	Cytoplasmic FMR1-interacting protein 1	CYFP1	6	4	19	19	25	43	-1.53515	0.004032
52	P47895	Aldehyde dehydrogenase family 1 member A3	AL1A3	8	1	40	30	0	2	4.926083	0
53	Q969P0	Immunoglobulin superfamily member 8	IGSF8	7	2	15	12	34	51	-2.96176	8.58E-05
54	P48594	Serpin B4	SPB4	4	4	61	41	2	2	5.949596	0
55	Q9NQS3	Nectin-3	NECT3	4	4	51	43	17	24	2.411158	8.58E-05
56	Q14160	Protein scribble homolog	SCRIB	5	3	16	13	60	77	-4.59944	0
57	P22223	Cadherin-3	CADH3	4	3	62	64	9	6	5.371313	0
58	P10644	cAMP-dependent protein kinase type I-alpha regulatory subunit	KAP0	3	4	9	12	2	3	1.799359	0.001802
59	O94973	AP-2 complex subunit alpha-2	AP2A2	5	2	19	11	23	43	-1.95715	0.001287
60	P05026	Sodium/potassium-transporting ATPase subunit beta-1	AT1B1	5	1	33	30	8	8	2.926488	8.58E-05
61	Q16658	Fascin	FSCN1	3	3	13	10	3	3	1.793849	0.001802

62	P55795	Heterogeneous nuclear ribonucleoprotein H2	HNRH2	4	2	12	12	3	5	1.578868	0.003174
63	P19256	Lymphocyte function-associated antigen 3	LFA3	3	3	21	18	8	10	1.502476	0.004204
64	P46939	Utrophin	UTRO	3	3	12	9	24	23	-1.69716	0.002745
65	Q9P2E9	Ribosome-binding protein 1	RRBP1	3	2	6	10	1	2	1.754103	0.002145
66	Q96PD2	Discoidin CUB and LCCL domain-containing protein 2	DCBD2	4	1	64	54	7	17	4.359452	0
67	P35221	Catenin alpha-1	CTNA1	2	3	19	12	3	4	2.216796	0.000601
68	P21399	Cytoplasmic aconitate hydratase	ACOC	3	2	7	10	2	2	1.637834	0.002745
69	Q99878	Histone H2A type 1-J	H2A1J	4	1	12	9	4	4	1.341385	0.006692
70	Q96KK5	Histone H2A type 1-H	H2A1H	4	1	12	9	4	4	1.341385	0.006692
71	P20671	Histone H2A type 1-D	H2A1D	4	1	12	9	4	4	1.341385	0.006692
72	P0C0S8	Histone H2A type 1	H2A1	4	1	12	9	4	4	1.341385	0.006692
73	Q9BTM1	Histone H2A.J	H2AJ	4	1	12	9	4	4	1.341385	0.006692
74	Q16777	Histone H2A type 2-C	H2A2C	4	1	12	9	4	4	1.341385	0.006692
75	Q6FI13	Histone H2A type 2-A	H2A2A	4	1	12	9	4	4	1.341385	0.006692
76	P30483	HLA class I histocompatibility antigen B-45 alpha chain	1B45	4	1	48	41	19	22	2.22212	0.000601
77	P30479	HLA class I histocompatibility antigen B-41 alpha chain	1B41	3	2	39	36	21	21	1.60275	0.002917
78	P31947	14-3-3 protein sigma	1433S	4	1	39	41	24	27	1.321577	0.006863
79	P16422	Epithelial cell adhesion molecule	EPCAM	4	1	60	64	33	53	1.346903	0.006606
80	P49915	GMP synthase [glutamine-hydrolyzing]	GUAA	4	1	14	12	36	41	-2.71245	8.58E-05
81	O43490	Prominin-1	PROM1	1	3	28	18	0	0	4.033175	0
82	P35613	Basigin	BASI	3	1	40	29	5	10	3.289321	0
83	P01701	Immunoglobulin lambda variable 1-51	LV151	2	2	41	32	5	15	3.012866	8.58E-05
84	P04899	Guanine nucleotide-binding protein G(i) subunit alpha-2	GNAI2	3	1	19	12	3	7	1.821503	0.001802
85	P62070	Ras-related protein R-Ras2	RRAS2	2	2	7	5	10	19	-1.45484	0.004461
86	P47929	Galectin-7	LEG7	3	0	25	16	0	0	3.761059	0
87	P16401	Histone H1.5	H15	0	3	6	4	0	0	1.369679	0.006005
88	Q9NYQ8	Protocadherin Fat 2	FAT2	2	1	5	4	0	0	1.2457	0.008065
89	Q14517	Protocadherin Fat 1	FAT1	3	0	19	18	0	1	3.530173	0
90	P13611	Versican core protein	CSPG2	1	2	23	21	2	2	3.487332	0
91	P00533	Epidermal growth factor receptor	EGFR	2	1	45	30	4	9	3.744261	0
92	O60437	Periplakin	PEPL	0	3	7	9	1	2	1.754103	0.002145
93	Q9ULT8	E3 ubiquitin-protein ligase HECTD1	HECD1	2	1	9	5	3	1	1.349604	0.006263
94	Q86W92	Liprin-beta-1	LIPB1	3	0	6	7	2	2	1.246193	0.008065
95	P50570	Dynamin-2	DYN2	3	0	6	3	10	14	-1.44686	0.00489

96	P09382	Galectin-1	LEG1	3	0	5	4	12	17	-1.80994	0.001802
97	Q15437	Protein transport protein Sec23B	SC23B	3	0	7	2	13	23	-2.26537	0.000515
98	Q8IWT6	Volume-regulated anion channel subunit LRRC8A	LRC8A	2	1	5	4	17	26	-2.67498	8.58E-05
99	O15479	Melanoma-associated antigen B2	MAGB2	2	0	6	6	0	0	1.598886	0.002917
100	Q9GZM7	Tubulointerstitial nephritis antigen-like	TINAL	2	0	6	6	0	0	1.598886	0.002917
101	O15427	Monocarboxylate transporter 4	MOT4	0	2	17	17	2	1	3.107601	8.58E-05
102	Q02952	A-kinase anchor protein 12	AKA12	1	1	5	4	0	1	1.2457	0.008065
103	P06400	Retinoblastoma-associated protein	RB	0	2	5	4	0	1	1.2457	0.008065
104	Q86SQ0	Pleckstrin homology-like domain family B member 2	PHLB2	1	1	5	4	1	0	1.2457	0.008065
105	Q9NZW5	MAGUK p55 subfamily member 6	MPP6	2	0	5	4	0	1	1.2457	0.008065
106	P08174	Complement decay-accelerating factor	DAF	1	1	21	18	2	5	2.715304	8.58E-05
107	Q9UN86	Ras GTPase-activating protein-binding protein 2	G3BP2	2	0	6	5	0	2	1.236546	0.008236
108	A0A0B4J1V1	Immunoglobulin heavy variable 3-21	HV321	1	1	30	29	4	7	3.254153	0
109	A0A0J9YX35	Immunoglobulin heavy variable 3-64D	HV64D	1	1	20	15	3	9	1.849652	0.00163
110	Q9UIW2	Plexin-A1	PLXA1	2	0	25	18	28	44	-1.41838	0.005148
111	P08581	Hepatocyte growth factor receptor	MET	2	0	15	11	21	25	-1.25487	0.009008
112	Q15942	Zyxin	ZYX	1	1	5	5	14	14	-1.61584	0.003003
113	P24666	Low molecular weight phosphotyrosine protein phosphatase	PPAC	2	0	3	3	7	11	-1.37844	0.006349
114	Q9Y6E0	Serine/threonine-protein kinase 24	STK24	1	1	3	3	10	11	-1.63419	0.002917
115	Q99569	Plakophilin-4	PKP4	1	1	8	7	30	34	-3.06733	8.58E-05
116	P42892	Endothelin-converting enzyme 1	ECE1	1	1	3	5	12	23	-2.33436	0.000343
117	P10909	Clusterin	CLUS	1	1	3	3	11	19	-2.30022	0.000515
118	Q04721	Neurogenic locus notch homolog protein 2	NOTC2	2	0	4	4	18	23	-2.69226	8.58E-05
119	Q16513	Serine/threonine-protein kinase N2	PKN2	2	0	5	2	24	31	-3.56707	0
120	Q9Y5S2	Serine/threonine-protein kinase MRCK beta	MRCKB	1	1	6	3	27	45	-4.07077	0
121	O43491	Band 4.1-like protein 2	E41L2	1	0	23	31	0	0	4.437238	0
122	Q99959	Plakophilin-2	PKP2	1	0	6	7	0	0	1.705721	0.002574
123	Q08209	Serine/threonine-protein phosphatase 2B catalytic subunit alpha isoform	PP2BA	0	1	4	4	0	0	1.114016	0.009695
124	Q99996	A-kinase anchor protein 9	AKAP9	0	1	7	6	0	0	1.705721	0.002574
125	P21589	5'-nucleotidase	5NTD	1	0	30	20	0	1	4.239568	0
126	Q8NEZ4	Histone-lysine N-methyltransferase 2C	KMT2C	0	1	6	6	0	1	1.598886	0.002917
127	O95613	Pericentrin	PCNT	0	1	6	5	1	0	1.487109	0.004204
128	O14763	Tumor necrosis factor receptor superfamily member 10B	TR10B	1	0	6	5	0	1	1.487109	0.004204
129	P01766	Immunoglobulin heavy variable 3-13	HV313	1	0	11	7	1	3	1.727699	0.002402

130	A0A0B4J1Y9	Immunoglobulin heavy variable 3-72	HV372	1	0	9	8	1	3	1.637834	0.002745
131	P55011	Solute carrier family 12 member 2	S12A2	0	1	7	4	1	2	1.236546	0.008236
132	O00592	Podocalyxin	PODXL	1	0	10	14	3	5	1.578868	0.003174
133	O75487	Glypican-4	GPC4	1	0	30	28	34	54	-1.28995	0.00755
134	Q9BZ29	Dedicator of cytokinesis protein 9	DOCK9	1	0	8	5	14	20	-1.67881	0.002745
135	Q9NQ88	Fructose-2 6-bisphosphatase TIGAR	TIGAR	1	0	2	3	7	9	-1.36103	0.006606
136	O75044	SLIT-ROBO Rho GTPase-activating protein 2	SRGP2	1	0	2	2	6	8	-1.3496	0.006863
137	O00506	Serine/threonine-protein kinase 25	STK25	1	0	2	2	7	7	-1.3496	0.006863
138	P06493	Cyclin-dependent kinase 1	CDK1	1	0	3	5	14	16	-2.00979	0.001115
139	P60981	Destrin	DEST	0	1	1	5	10	14	-1.87086	0.001544
140	P50995	Annexin A11	ANX11	1	0	1	2	3	9	-1.34893	0.006863
141	Q9UH65	Switch-associated protein 70	SWP70	1	0	2	1	6	7	-1.45634	0.004461
142	Q8IZ83	Aldehyde dehydrogenase family 16 member A1	A16A1	1	0	3	1	12	8	-1.89965	0.001287
143	Q86VI3	Ras GTPase-activating-like protein IQGAP3	IQGA3	0	1	6	3	17	30	-2.89292	8.58E-05
144	Q7L1W4	Volume-regulated anion channel subunit LRRC8D	LRC8D	0	1	2	2	19	26	-3.54153	0
145	P51511	Matrix metalloproteinase-15	MMP15	0	0	22	19	0	0	3.761059	0
146	Q52LW3	Rho GTPase-activating protein 29	RHG29	0	0	8	9	0	0	2.093743	0.000944
147	P15104	Glutamine synthetase	GLNA	0	0	6	6	0	0	1.598886	0.002917
148	P22413	Ectonucleotide pyrophosphatase/phosphodiesterase family member 1	ENPP1	0	0	10	7	0	0	2.093743	0.000944
149	Q96LD1	Zeta-sarcoglycan	SGCZ	0	0	15	21	0	0	3.470369	0
150	Q16585	Beta-sarcoglycan	SGCB	0	0	8	5	0	0	1.705721	0.002574
151	P08582	Melanotransferrin	TRFM	0	0	14	8	0	0	2.514426	8.58E-05
152	Q99988	Growth/differentiation factor 15	GDF15	0	0	13	14	0	0	2.88589	8.58E-05
153	Q9UBV4	Protein Wnt-16	WNT16	0	0	10	5	0	0	1.906764	0.001287
154	Q9UNN8	Endothelial protein C receptor	EPCR	0	0	25	25	0	0	4.239568	0
155	Q6ZMU5	Tripartite motif-containing protein 72	TRI72	0	0	6	3	0	0	1.2457	0.008065
156	Q14847	LIM and SH3 domain protein 1	LASP1	0	0	9	7	0	0	2.001838	0.001115
157	O43556	Epsilon-sarcoglycan	SGCE	0	0	13	14	0	0	2.88589	8.58E-05
158	Q9NZN4	EH domain-containing protein 2	EHD2	0	0	5	5	0	0	1.369679	0.006005
159	P50281	Matrix metalloproteinase-14	MMP14	0	0	9	5	0	0	1.80819	0.001802
160	O75326	Semaphorin-7A	SEM7A	0	0	5	4	0	0	1.2457	0.008065
161	Q8TCZ2	CD99 antigen-like protein 2	C99L2	0	0	3	5	0	0	1.114016	0.009695
162	P01008	Antithrombin-III	ANT3	0	0	5	3	0	0	1.114016	0.009695
163	O43688	Phospholipid phosphatase 2	PLPP2	0	0	4	4	0	0	1.114016	0.009695

164	Q02487	Desmocollin-2	DSC2	0	0	28	22	0	1	4.239568	0
165	P01699	Immunoglobulin lambda variable 1-44	LV144	0	0	7	10	0	1	2.093743	0.000944
166	P23470	Receptor-type tyrosine-protein phosphatase gamma	PTPRG	0	0	29	19	2	1	3.901046	0
167	P08648	Integrin alpha-5	ITA5	0	0	42	37	2	4	4.767191	0
168	P50748	Kinetochore-associated protein 1	KNTC1	0	0	5	6	0	1	1.487109	0.004204
169	P37840	Alpha-synuclein	SYUA	0	0	39	41	5	3	4.526349	0
170	Q5T2T1	MAGUK p55 subfamily member 7	MPP7	0	0	6	4	1	0	1.369679	0.006005
171	P01782	Immunoglobulin heavy variable 3-9	HV309	0	0	6	4	0	1	1.369679	0.006005
172	Q92817	Envoplakin	EVPL	0	0	7	11	2	0	1.936038	0.001287
173	P48960	CD97 antigen	CD97	0	0	12	6	0	2	1.936038	0.001287
174	P01024	Complement C3	CO3	0	0	5	3	0	1	1.114016	0.009695
175	P46783	40S ribosomal protein S10	RS10	0	0	4	4	1	0	1.114016	0.009695
176	Q9Y623	Myosin-4	MYH4	0	0	4	6	1	1	1.369679	0.006005
177	P13987	CD59 glycoprotein	CD59	0	0	6	6	0	3	1.138391	0.009094
178	P21709	Ephrin type-A receptor 1	EPHA1	0	0	12	6	3	2	1.544182	0.003861
179	P23471	Receptor-type tyrosine-protein phosphatase zeta	PTPRZ	0	0	6	4	2	1	1.118495	0.009695
180	O60353	Frizzled-6	FZD6	0	0	6	7	2	2	1.246193	0.008065
181	P22694	cAMP-dependent protein kinase catalytic subunit beta	KAPCB	0	0	6	6	3	1	1.138391	0.009094
182	Q9Y639	Neuroplastin	NPTN	0	0	13	11	2	7	1.446863	0.004547
183	P54709	Sodium/potassium-transporting ATPase subunit beta-3	AT1B3	0	0	24	22	9	14	1.482623	0.004204
184	Q6P1M3	Lethal(2) giant larvae protein homolog 2	L2GL2	0	0	15	17	30	26	-1.35393	0.006606
185	P42356	Phosphatidylinositol 4-kinase alpha	PI4KA	0	0	8	6	10	21	-1.37935	0.005748
186	Q96J02	E3 ubiquitin-protein ligase Itchy homolog	ITCH	0	0	6	6	13	15	-1.38489	0.005748
187	Q9NY35	Claudin domain-containing protein 1	CLDN1	0	0	3	2	6	9	-1.2648	0.008236
188	Q9Y666	Solute carrier family 12 member 7	S12A7	0	0	1	3	5	8	-1.24619	0.009094
189	Q8N3E9	1-phosphatidylinositol 4 5-bisphosphate phosphodiesterase delta-3	PLCD3	0	0	5	3	13	15	-1.87181	0.001458
190	P04818	Thymidylate synthase	TYSY	0	0	1	3	4	10	-1.3496	0.006863
191	Q9Y2X7	ARF GTPase-activating protein GIT1	GIT1	0	0	1	2	4	8	-1.34893	0.006863
192	Q14156	Protein EFR3 homolog A	EFR3A	0	0	4	2	11	15	-2.01985	0.001115
193	Q9NQX4	Unconventional myosin-Vc	MYO5C	0	0	1	3	5	13	-1.7277	0.002402
194	Q96RF0	Sorting nexin-18	SNX18	0	0	2	2	7	11	-1.7277	0.002402
195	Q8WXE0	Caskin-2	CSKI2	0	0	1	1	4	5	-1.2457	0.009351
196	Q4KMP7	TBC1 domain family member 10B	TB10B	0	0	2	1	5	9	-1.55938	0.003689
197	Q9H2G2	STE20-like serine/threonine-protein kinase	SLK	0	0	7	4	21	33	-3.01267	8.58E-05

198	**Q12965**	**Unconventional myosin-Ie**	**MYO1E**	**0**	**0**	**2**	**3**	**13**	**12**	**-2.11059**	**0.000858**
199	**P10301**	**Ras-related protein R-Ras**	**RRAS**	**0**	**0**	**1**	**1**	**3**	**7**	**-1.36968**	**0.006606**
200	**O76003**	**Glutaredoxin-3**	**GLRX3**	**0**	**0**	**1**	**1**	**5**	**5**	**-1.36968**	**0.006606**

Proteins that fulfilled the screening criteria ([1] the estimated amount of the protein in the anti CD147-HRP labeled sample was at least five times more than that in the anti huIgG-HRP labeled sample; [2] the protein fulfilled criterion in two independent replicates *p.p*:* proximal partners of CD147, *STN* :* Signal to noise ratio generated by PLGEM

3.2 Surface assembly of CD147 lateral interactome in the lipid raft microdomain in CSCs

We and others have demonstrated that CD147and EGFR partially localize in a membrane lipid raft microdomain in malignant cancer cells[8]. Thus, we investigated cellular compartmentalization of selected CD147 proximal proteins within the lipid rafts in CSC and compared with NCSC. To evaluate the sequestration of identified proximal proteins together with CD147 within the lipid raft microdomain, we first examined whether CD147 was localized in the lipid raft microdomain or not. We found that CD147 was detected in the caveolin-enriched lipid raft microdomain (~20% Optiprep™) of CSCs. Treatment of CSCs with MBCD resulted in a disappearance in CD147 levels, while there was no CD147 localized in NCSCs and CD147KO CSCs suggested that sequestration of CD147 into the microdomain in CSCs is an important surface phenotype of CSCs **(Figure 7A)**.

Previously, Grass *et. al*. reported that CD147, CD44 and EGFR formed complexes in MDA-MB231 cells[9]. We also investigated whether CD147 formed cell surface assembly with CD44 and EGFR including CD133, CD276 and MCT4 within the lipid raft microdomain of CSCs and compared with NCSCs. Western blot analysis of both lipid raft (20% Optiprep™ density gradient) and non-lipid raft fractions (35% Optiprep™ density gradient) of CSCs and NCSCs. We found that the most of proteins were abundantly co-localized only in the lipid raft fraction of CSCs, not in NCSCs. The majority of proteins except EGFR were less abundant in the non-raft fraction of CSC, whereas CD276 was not detected at all, suggested that sequestration of oncogenic proteins including the immune checkpoint molecule may be the intrinsic cell surface molecular properties of CSCs **(Figure 7B)**.

3.3 CD147-mediated CD147 lateral assembly in CSCs

To further demonstrate that CD147 is the main factor that causes its proximal proteins to recruit in the lipid rafts, we performed systematic western-blot analysis of lipid raft fractions of single KO cell lines (CD147KO, CD44KO, CD133KO) including a double KO cell line (CD147/CD44) and a triple KO cell line (CD147/CD44/CD133) of lipid rafts isolated from different Optiprep™ gradient conditions (15, 25 and 35%) **(Figure 8A)**. Western blots indicate expression levels of raft and non-raft fractions from each cell lines. We evaluated the levels of representation of CSC-specific proximal protein did not differ significantly in CD44KO_CSC and CD133KO_CSC **(Figure 8B)** although the level of CSC-specific proximal protein on the lipid raft decreased relatively in double KO (CD147/44) and triple KO_CSC (CD147/44/133) including CD147KO_CSC) **(Figure 8D)**. In particular, CD276 and MCT4 were significantly reduced in the CD147 KO series whereas there were no significant changes in CD44 and CD133 KO cell lines **(Figure 8C and E)**. Our data suggest that CD147 rather than any other proximal protein acts as the largest driving source in the making of the raft-assembly of CD147.

3.4 Co-localization of CD147 and CD276 in CSC lateral interactome in the lipid raft microdomain in CSCs

Among the proteins in surface assembly of CD147, surprising finding was the detection of CD276. The original description of CD276 indicated an immune checkpoint protein, participated in the regulation of T-cell mediated immune response. Any correlation between CD147 and CD276 has previously been described. Thus, to verify that CD276 is a component of surface assembly of CD147, we isolated the lipid raft from the CSC-CD276 KO cell line and probed with CD147 protein by western blot **(Figure 9B)** although there is no significant change in whole lysate from CSC and CSC-CD276KO cell line **(Figure 9A)**. The expression level of CD147 in the lipid raft was less abundance in CSC-CD276 KO cell line. To evaluate whether lateral interaction between CD147-CD276, we employed a PLA technique that detects associations of proteins occurring within 40nm of each other. We found that there were significant difference between CSC and MBCD treated CSC in regard to the percentage of the cell population demonstrating close associations of CD147 with CD276 **(Figure 9C)**.

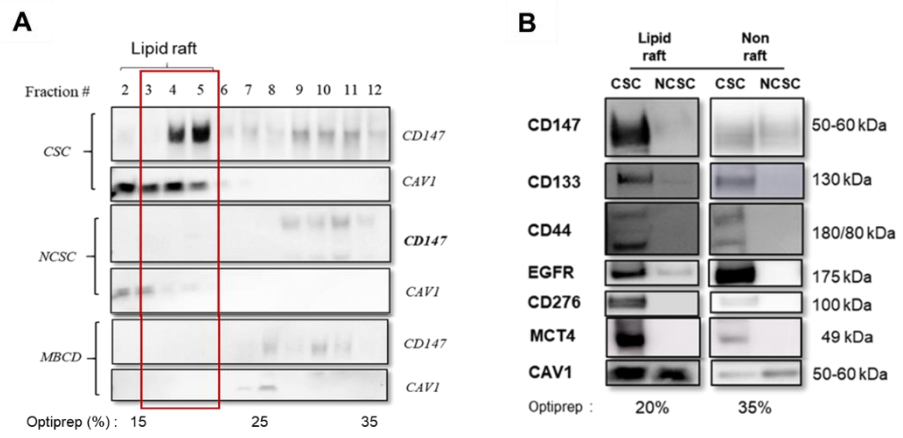

Figure 7. Surface Assembly of CD147 and Proximal Proteins in raft-like microdomain. Cells were homogenized in a detergent containing lysis buffer and were subsequently brought to a discontinuous iodixanol gradient (4 hours, 4°C, 200,000 x g in a Beckman SW41 Ti rotor). After ultracentrifugation, fractions were collected and analysed for CD147 and caveolin-1, a lipid raft marker, by Western blot. The red box indicates lipid raft fractions. **(A)** Lipid rafts isolation from CSCs, NCSCs, and including MBCD treated CSC. **(B)** 20ug of raft fractions and non-raft fractions from CSC and NCSC were separated by SDS-PAGE under non-reducing conditions, and blotted for CD147, proximal proteins (CD133, CD44, EGFR, MCT4 and CD276) and Cav-1. Surface Assembly of CD147 and Proximal Proteins in raft-like microdomain.

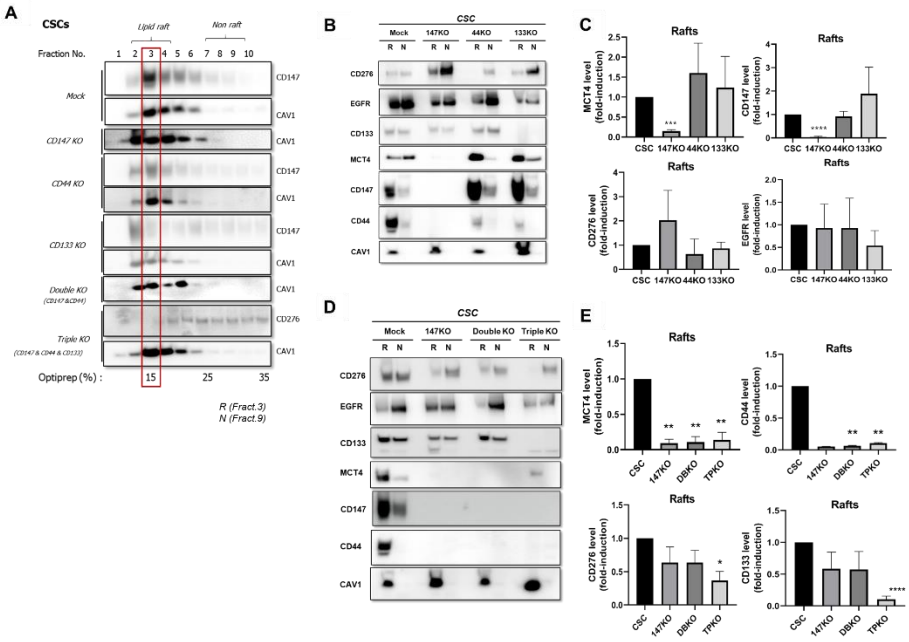

Figure 8. CD147 mediated cell surface assembly in CSCs. (A) Lipid rafts isolation from CSCs, CD147 KO-CSC, CD44 KO-CSC, CD133 KO-CSC, CD147/CD44 double KO-CSC (DBKO), CD147/CD44/CD133 triple KO-CSC (TPKO). The red box indicates lipid raft fractions. **(B)** Western blot analysis for the expression of proximal proteins of CD147 in lipid raft fraction and non-raft fraction in the CD147 KO, CD44 KO, and CD133 KO with control in CSC. **(C)** Quantitative analysis of the ratio of the relative fold increase over the control for CD276 and MCT4. **(D)** Western blot analysis for the expression of proximal proteins of CD147 in lipid raft fraction and non-raft fraction in the CD147 KO, DBKO, and TPKO with control in CSC. **(E)** Quantitative analysis of the raft of the relative fold increase over the control for CD147 and MCT4. The results represent the mean value of three independent experiments. *P<0.05 vs the control.

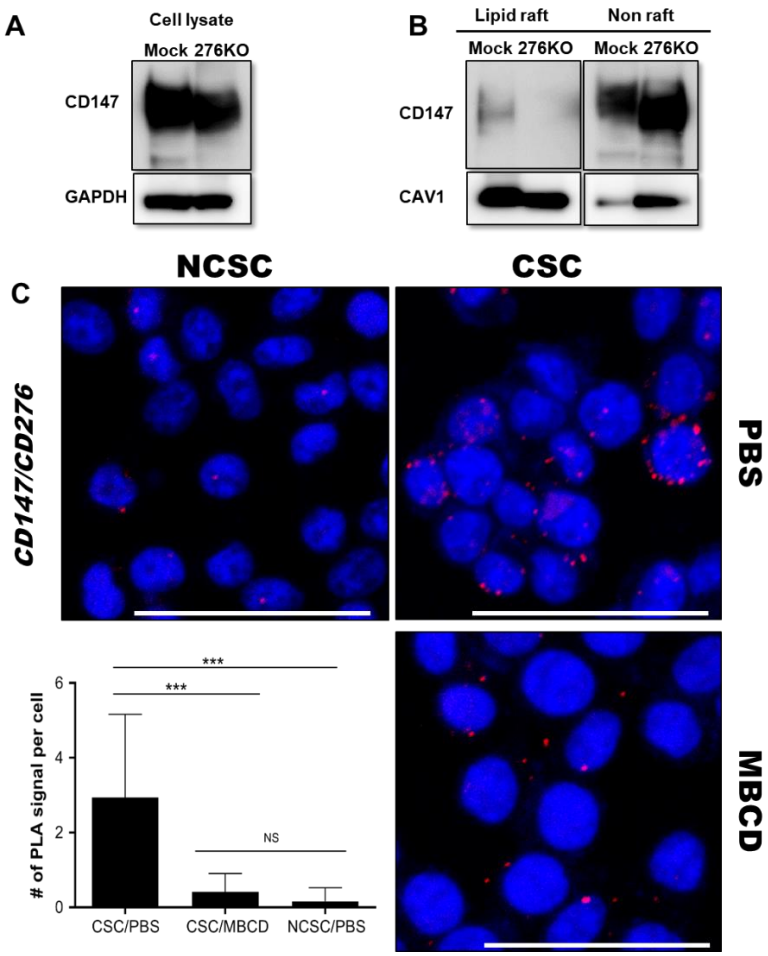

Figure 9. The CD276 have close-interaction with CD147 in CSC lateral interactome in the lipid raft microdomain in CSCs. Western blot of CD2147 protein in whole cell lysates **(A)** and both lipid raft and non-raft fractions **(B)** in CSC and CD276 KO-CSC. Each lane was loaded with 20ug protein of cell lysate and raft and non-raft fractions and separated under non-reducing conditions, and blotted for CD147 with GAPDH or CAV1. **(C)** PLA signal and its quantification between CD147 and CD276 in CSC and NCSC with MBCD treatment or not. *Bar = 10um.*

3.5 Surface assembly of CD147 lateral interactome is associated with resistance phenotype to docetaxel in CSC

Given that CSCs have a crucial role not only in cancer metastasis, but also associate with anticancer drug resistance and tumor initiation, we further studied anticancer drug resistance sustainability of CSC related to the assembly of CD147 lateral interactome in the cell surface of CSC **(Figure 10A)**. Therefore, we asked whether MBCD may sensitizes tumors to docetaxel therapy as disrupting the surface assembly of CD147 lateral interactome in CSC treatment**.** To this end, CSC and CSC-CD147KO were treated with MBCD and/or docetaxel **(Figure 10B).** Cell viability was monitored. As depicted in **Figure 10C**, MBCD treated CSCs shown that the survival levels to docetaxel were significantly decreased, whereas the proliferation of both CSC and CSC-CD147KO cells was not affected by the MBCD treatment only. However, CSC-CD147KO cells exhibited docetaxel sensitive in the condition of MBCD treatment or not and the rate of docetaxel resistance of parental cells sustained similar to that of the CD147KO cells, suggesting that MBCD induced disruption of surface assembly of CD147 allow to reverse the resistance phenotype to sensitive.

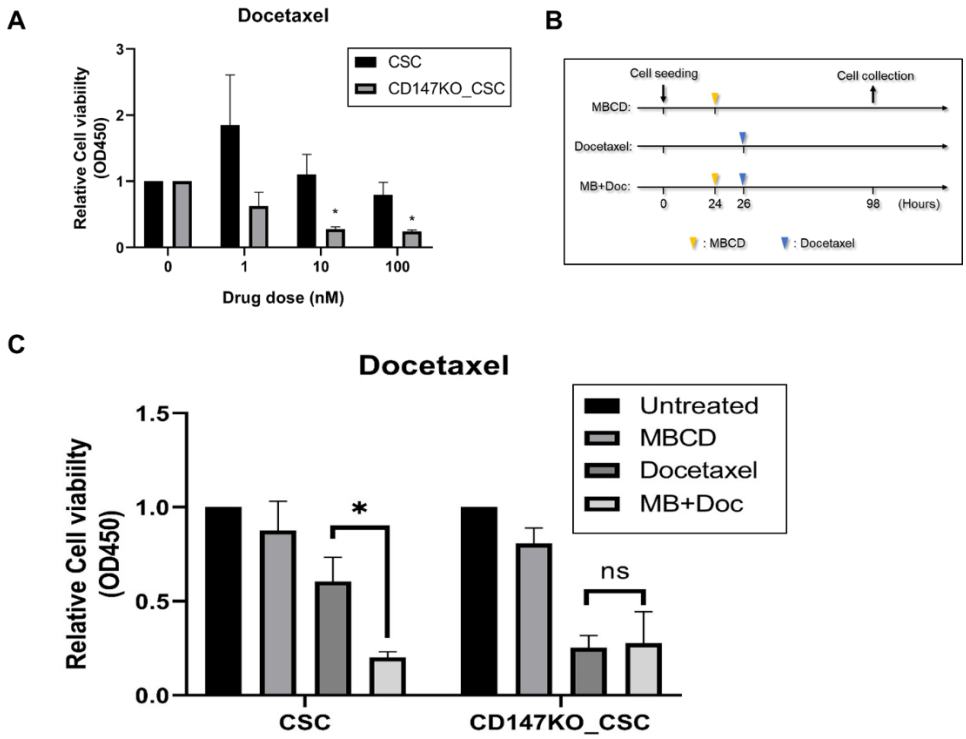

Figure 10. Effects of docetaxel on viability of surface assembly of CD147 and its proximal proteins in lipid raft like domain. (A) CSC and CD147KO-CSC were incubated in 100uL of medium for 24 h and then treated with docetaxel at the indicated concentrations. After 72 h of treatment, the cell viabilities were measured via EZ-cytox assay kit (n=3). The percentage of viable cells is shown relative to that of untreated controls. **(B)** Schematic diagram illustrating the treatment protocol of methyl-beta cyclodextrin (MBCD) and/or 25 nM docetaxel (Doc) in CSC and CD147 KO CSC. **(C)** Cells were exposed to medium containing 5mM MBCD for 2 h, and then incubated in fresh medium with or without 25nM docetaxel for 72 h. Subsequently, cell viability was measured.

3.4 Docetaxel inhibits cell cycle progression at the subG1 phase in CSCs by disrupting surface assembly of CD147

To better understand the mechanism of surface assembly of CD147 in inhibited cell proliferation, the study further analyzed the effects of docetaxel on cell cycle distribution due to the presence or absence of surface assembly structure in CSC and CD147 KO_CSC by flow cytometry **(Figure 11A).** In CSC, the number of apoptotic cells in SubG1 shows combination treatment of MBCD and docetaxel were significantly induced apoptotic levels compared to docetaxel treated alone **(Figure 11B)**. Unlike the CSCs, CSC-CD147 KO indicates that the resistance phenotype to docetaxel is lost regardless of the disruption of surface assembly. These data indicated that disrupted CD147 assembly followed by docetaxel treatment may modulate Sub G1 transition in the cell cycle progression of CSCs. The cell cycle process is well known to be controlled by several types of cyclins, CDKs and CDK inhibitors (CDKI). To explain the molecular mechanism by which disrupted assembly followed by docetaxel treatment induced apoptosis, the expression of various cycle process proteins were detected. The results demonstrated that the protein expression levels of cell cycle promoter, cyclin A, was markedly decreased, whereas the expression levels of CDKIs, p53, were significantly upregulated **(Figure 11C).**

The serine-threonine protein kinase AKT1 (Akt) has been reported to be closely associated with the proliferation of tumor cells (ref). Survival factors can suppress apoptosis in a transcription-independent manner by activating the serine/threonine kinase AKT1, which then phosphorylates and inactivates components of the apoptotic machinery. Therefore, this study examined the alteration in Akt and phosphorylation on ser 473 **(Figure 12).** These findings indicated that docetaxel may slow cell cycle progression by downregulating interrelated cyclin A and CDKs modulated by Akt in the event of a malfunction in the CD147 assembly.

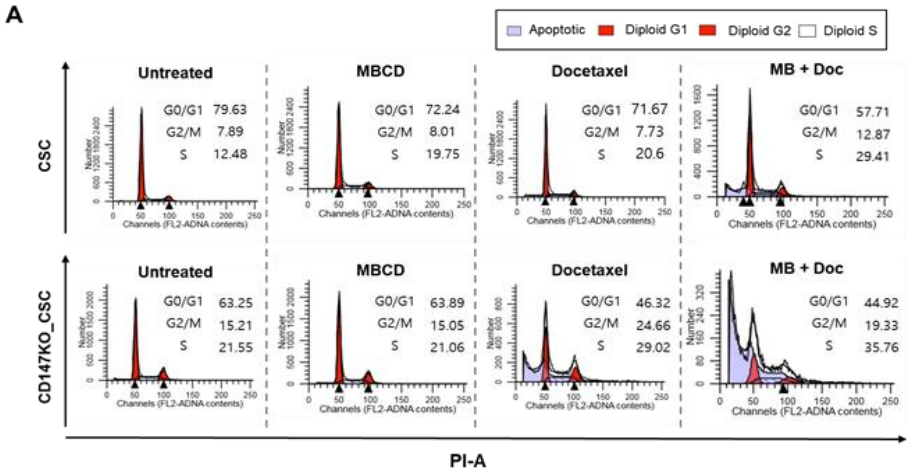
A
Apoptotic
Diploid G1
Diploid G2
Diploid S
CSC
CD147KO_CSC
Untreated
MBCD
Docetaxel
MB + Doc
G0/G1 79.63
G2/M 7.89
S 12.48
G0/G1 72.24
G2/M 8.01
S 19.75
G0/G1 71.67
G2/M 7.73
S 20.6
G0/G1 57.71
G2/M 12.87
S 29.41
G0/G1 63.25
G2/M 15.21
S 21.55
G0/G1 63.89
G2/M 15.05
S 21.06
G0/G1 46.32
G2/M 24.66
S 29.02
G0/G1 44.92
G2/M 19.33
S 35.76
Channels (FL2-ADNA contents)
PI-A

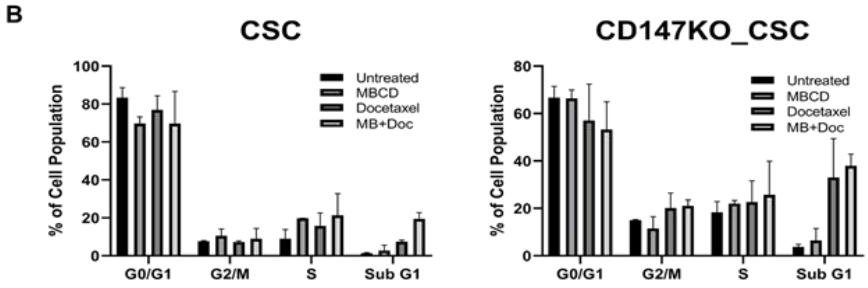
B
CSC
CD147KO_CSC
% of Cell Population
Untreated
MBCD
Docetaxel
MB+Doc
G0/G1
G2/M
S
Sub G1

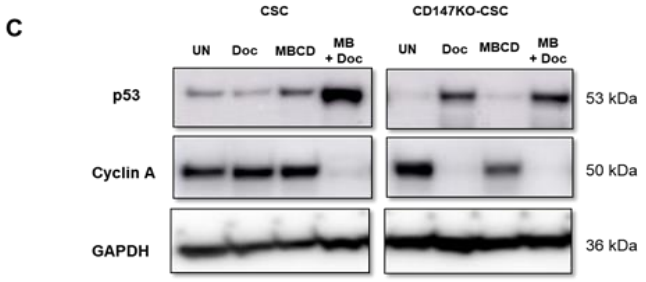
C
CSC
CD147KO-CSC
UN
Doc
MBCD
MB + Doc
p53
Cyclin A
GAPDH
53 kDa
50 kDa
36 kDa

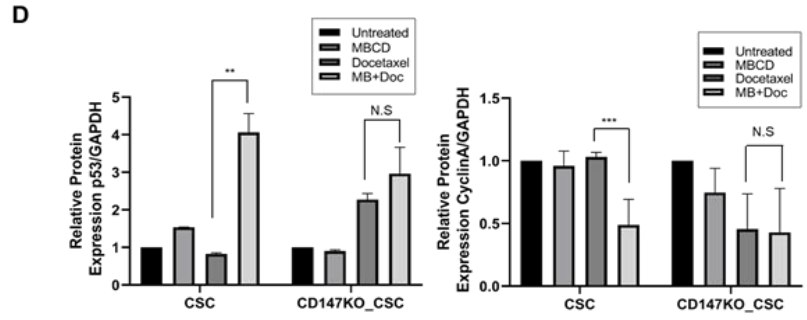
D
Untreated
MBCD
Docetaxel
MB+Doc
Relative Protein Expression p53/GAPDH
Relative Protein Expression CyclinA/GAPDH
**
***
N.S
CSC
CD147KO_CSC

Figure 11. Involvement the surface assembly to docetaxel in the cell cycle arrest. CSC and CSC-CD147 KO cells were treated with 5mM MBCD for 2 h and then treated with 25nM docetaxel for 72 h. Harvested cells were washed using cold PBS and fixed with ice-cold 70% ethanol for 4h at 4°C. Fixed cells were washed PBS, followed by staining with propidium iodide (PI). **(A and B)** Flow cytometric analysis and quantification of the cell cycle progression in CSC and CD147 KO cells treated with 5mM MBCD for 2 h and then treated with 25nM docetaxel (Doc) for 72 h. **(C and D)** Western blot and quantification reveled that cells treated with MBCD and Docetaxel affected the expression of cell cycle related proteins, including cyclin A and p53. GAPDH was used as a loading control.

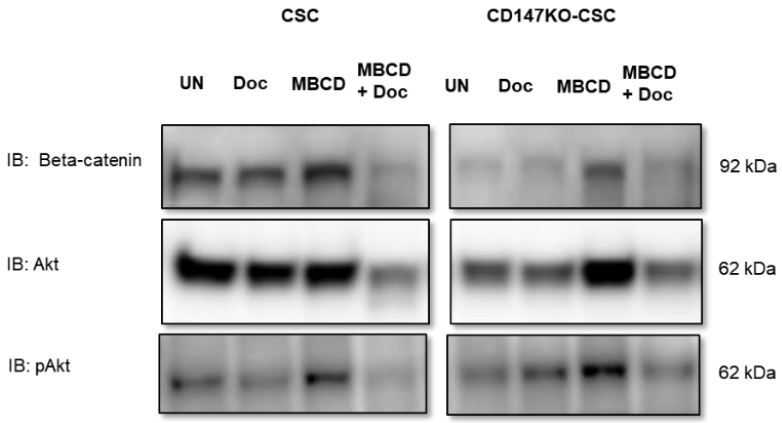

Figure 12. Inhibitory effects of lipid raft disruption on phosphorylation of beta-catenin axis phospho Akt signaling. CSC and CSC-CD147 KO cells were treated with 5mM MBCD for 2 h and then treated with 25nM docetaxel for 72 h. Immunoblotting using Akt, phospho-Akt, and beta-catenin antibodies was performed as described. Immunoblots are representative of at least three independent experiments.

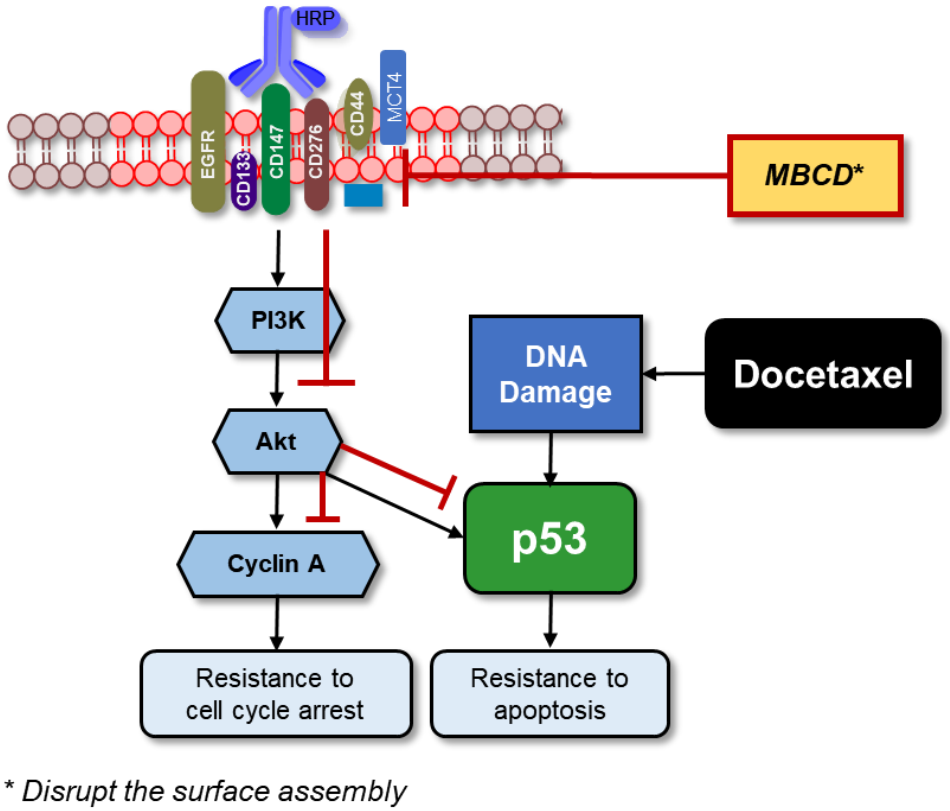

Figure 13. Proposed mechanism underlying an inhibitory effect of disrupting lipid raft domain on aggressive cancer stem cells.

4. Discussion

I and others have demonstrated that CD147 confers chemoresistance phenotype in breast cancer stem cells[4] although the exact signaling mechanisms regulating these processes and which protein compositions are interacting are not well understood. Proximity labeling technique is playing a growing role in this endeavor, as it can identify proximal partners that can be difficult to capture by other methods[21]. Here, we adopted to deposit a biotin label into CD147 nearest surface-localized protein assemblies on live cells and biotinylated proteins recovered by affinity purification for their identification by tandem MS. This approach provides available strategies to CD147 thereby identify co-localized proteins in this complex system for understanding tumor microenvironment.

I identified CD133, CD44, EGFR and integrin family which are previously implicated in the regulation of cancer stemness with CD147[4]. Among the proximal partners with CD147 in CSCs, a surprising finding is that the functional annotation indicates these proteins are associated in regulating specific microdomain. Moreover, *G. Daniel Grass* noted that CD147, as well as CD44 and EGFR, are present in lipid raft fractions in breast cancer cells, but interactions between these proteins clearly occur in these cells. So, he suggested strongly that a small but critical subfraction of CD147 is distributed along with its binding partners in these structures. It should be noted that the conceptually similar proximity labeling assay that targeted raft microdomain components. A number of reports have demonstrated that CD147 is present in lipid rafts[8]. These study indicate a close association of surface assembly of CD147 within raft microdomain. A characteristic feature of cell surface assembly with CD147 is that proteins residing together in the raft microdomain. It makes easier to demonstrate the close co-assembly of CD147 with identified proximal proteins.

Interaction between CD147 and its nearest assembly is related to the cancer stem cell properties which are associated with their resistance to current clinical cancer

therapies[22]. Sajithlal et al. studied differential chemotherapeutic sensitivities and found that the CSC-like cells were resistant to adriamycin, etoposide, 5-FU, and docetaxel. Docetaxel is widely used in the treatment of breast cancers. The chemotherapy agent for docetaxel, which interferes with depolymerizing microtubule, induced microtubule stabilization arrests cells in the G(2)M phase of the cell cycle and induces bcl-2 phosphorylation, thereby promoting a cascade of events that ultimately leads to apoptotic cell death[23].

Furthermore, our data suggest that disruption of surface assembly via MBCD can sensitize cells to apoptotic stimuli in a CSC-like cells. In this regard, we have shown that disruption of surface assembly of CD147 synergizes with docetaxel in chemo-resistant breast cancer cell lines. Specifically, co-treatment of these cell lines with MBCD and docetaxel significantly induces cell cycle arrest compared to either drug alone (Figure 9A). Thus, in breast cancer cells resistant to chemo-reagent, CD147 is commonly localized to lipid rafts[8], and our data indicate that this localization plays a functional role in such resistance.

Localization of CD147 to lipid rafts with constituting the surface assembly is an important factor in the resistance of breast cancer cells to docetaxel-induced growth inhibition. Our data suggest that the synergistic mechanism between MBCD and docetaxel in breast cancer cells is due to depletion of lipid rafts and thereby disruption of surface assembly. Thus, MBCD sensitized docetaxel resistance breast cancer cells to induced apoptotic signaling. Importantly, this sensitization of docetaxel resistance cells was determined to be synergistic although there is no significant change in CD147 knockout CSC with MBCD treatment. We hypothesize that lipid rafts provide the surface assembly by which CD147 interacts with other oncogenic proximal proteins and activate signaling pathways including the Akt pathway.

In summary, we have described the cell surface assembly of CD147 in CSC tumor microenvironment by implementing in-situ proximity labeling method. The proximal

partners of CD147 may provide valuable information for the resistance phenotype of cancer therapies. Our data suggest the surface assembly of CD147 might be one of the critical oncogenic membrane proteins involved in promoting chemoresistance and cell survival in CSC-like cells, and that disruption of the surface assembly may explain its importance in CSC biology. The surface assembly of the CD147 is dynamic, and its composition may confer the cancer stemness with oncogenic phenotype. Based on the successful identification of proteins known to be functionally associated with the resistance phenotype to chemo-reagent. On top of that, we further described the close-interaction between CD147 and CD276 has specific contribution to cancer stemness. Further studies are needed to define the physiological roles between CD147 and CD276 in conferring CSC-specific chemo-resistance phenotype.

5. References

1 Luschnig, C. & Vert, G. The dynamics of plant plasma membrane proteins: PINs and beyond. *Development* **141**, 2924-2938, doi:10.1242/dev.103424 (2014).

2 Zhou, S. *et al.* CD147 mediates chemoresistance in breast cancer via ABCG2 by affecting its cellular localization and dimerization. *Cancer Lett* **337**, 285-292, doi:10.1016/j.canlet.2013.04.025 (2013).

3 Nabeshima, K. *et al.* Emmprin (basigin/CD147): matrix metalloproteinase modulator and multifunctional cell recognition molecule that plays a critical role in cancer progression. *Pathol Int* **56**, 359-367, doi:10.1111/j.1440-1827.2006.01972.x (2006).

4 Kang, M. J. *et al.* Proteomic analysis reveals that CD147/EMMPRIN confers chemoresistance in cancer stem cell-like cells. *Proteomics* **13**, 1714-1725, doi:10.1002/pmic.201200511 (2013).

5 Khayati, F. *et al.* EMMPRIN/CD147 is a novel coreceptor of VEGFR-2 mediating its activation by VEGF. *Oncotarget* **6**, 9766-9780, doi:DOI 10.18632/oncotarget.2870 (2015).

6 Toole, B. P. & Slomiany, M. G. Hyaluronan, CD44 and Emmprin: Partners in cancer cell chemoresistance. *Drug Resist Update* **11**, 110-121, doi:DOI 10.1016/j.drup.2008.04.002 (2008).

7 Grass, G. D., Dai, L., Qin, Z. Q., Parsons, C. & Toole, B. P. CD147: Regulator of Hyaluronan Signaling in Invasiveness and Chemoresistance. *Adv Cancer Res* **123**, 351-373, doi:10.1016/B978-0-12-800092-2.00013-7 (2014).

8 Grass, G. D., Tolliver, L. B., Bratoeva, M. & Toole, B. P. CD147, CD44, and the Epidermal Growth Factor Receptor (EGFR) Signaling Pathway Cooperate to Regulate Breast Epithelial Cell Invasiveness. *Journal of Biological Chemistry* **288**, 26089-26104, doi:10.1074/jbc.M113.497685 (2013).

9 Hao, J. L., Cozzi, P. J., Khatri, A., Power, C. A. & Li, Y. CD147/EMMPRIN and CD44 are Potential Therapeutic Targets for Metastatic Prostate Cancer. *Curr Cancer Drug Tar* **10**, 287-306, doi:Doi 10.2174/156800910791190193 (2010).

10 Chang, L. Y. *et al.* Identification of Siglec Ligands Using a Proximity Labeling Method. *J Proteome Res* **16**, 3929-3941, doi:10.1021/acs.jproteome.7b00625 (2017).

11 Hung, V. *et al.* Proteomic Mapping of the Human Mitochondrial Intermembrane Space in Live Cells via Ratiometric APEX Tagging. *Mol Cell* **55**, 332-341, doi:10.1016/j.molcel.2014.06.003 (2014).

12 Kotani, N. *et al.* Biochemical visualization of cell surface molecular clustering in living cells. *P Natl Acad Sci USA* **105**, 7405-7409, doi:10.1073/pnas.0710346105 (2008).
13 Li, X. W. *et al.* New Insights into the DT40 B Cell Receptor Cluster Using a Proteomic Proximity Labeling Assay. *Journal of Biological Chemistry* **289**, 14434-14447, doi:10.1074/jbc.M113.529578 (2014).
14 Roux, K. J., Kim, D. I., Raida, M. & Burke, B. A promiscuous biotin ligase fusion protein identifies proximal and interacting proteins in mammalian cells. *J Cell Biol* **196**, 801-810, doi:10.1083/jcb.201112098 (2012).
15 Sajithlal, G. B. *et al.* Permanently Blocked Stem Cells Derived From Breast Cancer Cell Lines. *Stem Cells* **28**, 1008-1018, doi:10.1002/stem.424 (2010).
16 Liu, Y. S. *et al.* Is the clinical malignant phenotype of prostate cancer a result of a highly proliferative immune-evasive B7-H3-expressing cell population? *Int J Urol* **19**, 749-756, doi:10.1111/j.1442-2042.2012.03017.x (2012).
17 Liu, Z. X. *et al.* Immunoregulatory protein B7-H3 regulates cancer stem cell enrichment and drug resistance through MVP-mediated MEK activation. *Oncogene* **38**, 88-102, doi:10.1038/s41388-018-0407-9 (2019).
18 Sun, J. *et al.* Clinical significance and regulation of the costimulatory molecule B7-H3 in human colorectal carcinoma. *Cancer Immunol Immun* **59**, 1163-1171, doi:10.1007/s00262-010-0841-1 (2010).
19 Yamato, I. *et al.* Clinical importance of B7-H3 expression in human pancreatic cancer. *Brit J Cancer* **101**, 1709-1716, doi:10.1038/sj.bjc.6605375 (2009).
20 Li, Z. Y. *et al.* Downregulation of caveolin-1 increases the sensitivity of drug-resistant colorectal cancer HCT116 cells to 5-fluorouracil. *Oncol Lett* **13**, 483-487, doi:10.3892/ol.2016.5390 (2017).
21 Samavarchi-Tehrani, P., Abdouni, H., Samson, R. & Gingras, A. C. A Versatile Lentiviral Delivery Toolkit for Proximity-dependent Biotinylation in Diverse Cell Types. *Mol Cell Proteomics* **17**, 2256-2269, doi:UNSP TIR118.000902
10.1074/mcp.TIR118.000902 (2018).
22 Mimeault, M. & Batra, S. K. New promising drug targets in cancer- and metastasis-initiating cells. *Drug Discov Today* **15**, 354-364, doi:10.1016/j.drudis.2010.03.009 (2010).
23 Pienta, K. J. Preclinical mechanisms of action of docetaxel and docetaxel combinations in prostate cancer. *Semin Oncol* **28**, 3-7, doi:10.1053/sonc.2001.26892 (2001).

6. Abstract in Korean

유방암 줄기세포에서 CD147 과 CD276 의 막단백질 집합체에 의한 항암제 저항성 기전 연구

세포막 단백질은 다양한 세포 사건을 조절하는 내생적, 환경적 단서에 대한 반응을 중재할 뿐만 아니라 세포 상태의 내적 특성을 유지한다. 여기서는 세포막에 존재하는 CD147 을 포함한 종양을 유발하는 단백질들의 어셈블리에 이 유방암 줄기 세포의 특징을 유지하는 데 필수적이라는 것을 보여 주는 것을 목표로 했다. 유방암 줄기세포에서 CD147 주변부 단백질을 CD276 과 CD44, CD133, EGFR 과 같이 CD147 의 가장 가까운 이웃으로 간주되는 알려진 암 줄기 세포 표지를 발견했다. CD147, CD276 및 기타 종양 발생 단백질들의 세포 표면 조립은 지질 뗏목이라는 특정 마이크로 도메인에서 종양 미세환경을 이루는 것을 확인했다. 고유한 표면 단백질 어셈블리의 시퀀스는 Akt 의존성 p53 매개 세포사멸 신호 경로를 통해 docetaxel 에 대한 저항을 제공한다. 요약하면 CD147 과 근위부 단백질 사이의 측간 상호작용은 docetaxel 저항을 촉진하고 암세포 줄기성 표현형의 주요 결정요인을 제시한다.